Analytical modelling and characterisation of an infrasound generator in the air

P. Vincent, F. Larsonnier, Dominique Rodrigues, Stéphane Durand

Applied Acoustics 148 (2019) 476–483

Contents lists available at ScienceDirect

Applied Acoustics

journal homepage: www.elsevier.com/locate/apacoust

Analytical modelling and characterisation of an infrasound generator in the air

P. Vincent [a], F. Larsonnier [a], D. Rodrigues [b], S. Durand [c]

[a] Commissariat à l'Énergie Atomique (CEA), DAM, DIF, F-91297 Arpajon, France
[b] Laboratoire Commun de Métrologie LNE-CNAM (LCM), 29 Avenue Roger Hennequin, 78197 Trappes Cedex, France
[c] Laboratoire d'Acoustique de l'Université du Mans (LAUM), UMR CNRS 6613, Avenue Olivier Messiaen, 72085 Le Mans Cedex 9, France

ARTICLE INFO

Article history:
Received 22 March 2018
Received in revised form 24 November 2018
Accepted 19 December 2018
Available online 18 January 2019

Keywords:
Infrasound
Generator
Microbarometer
Calibration
Genetic algorithm

ABSTRACT

This paper presents an accurate characterisation based on an experimental set-up and mathematical models of a dynamic pressure infrasound generator. The Commissariat à l'énergie atomique (CEA) has developed microbarometers to measure infrasound waves in the atmosphere. To characterise its sensors and validate their requirements, an infrasound generator has been designed, which covers a frequency range from 4.0 10^{-4} Hz to 300 Hz. This pressure generator still needs accurate characterisation as there is no standard reference in the infrasound frequency range for such sensor calibration. The research focused on 17 parameters that affect the behaviour of this infrasound pressure generator. Two analytical models of the sound pressure in the cylindrical cavity of the calibrator are presented. An experimental characterisation was also performed to adjust the model parameters with genetic algorithms to the measurements, and the results of the comparison between the measurements and the models are discussed. This study highlights the influence of the thermodynamic transition from isothermal to adiabatic transformation and the influence of viscoelastic non-linearities of a loudspeaker membrane. It aims to characterise the amplitude and phase responses of the generator in order to develop an improved infrasound calibration device for microbarometers with a similar technology.

1. Introduction

1.1. Context

The propagation of infrasonic waves in the air is used to characterise both natural and human related sources, from tsunamis [1] or volcanoes [2] in the mHz frequency range to the wind turbines [3], avalanches [4] or transportation [5,6] near the audio range. Confidence in the measurement of the sound pressure level of these sources is crucial to understand our environment and establish legal acceptance levels. The International Monitoring System (IMS) is a global detection network of geophysical stations managed by the Comprehensive Nuclear Test Ban Treaty Organization (CTBTO). This network is established all around the world in order to provide global coverage for the surveillance of nuclear testing. It uses hydro-acoustic, seismic and radionuclide monitoring, as well as measurement of infrasonic sound pressure in atmosphere, which is done with microbarometers. These instruments must respond to specific requirements, particularly in terms of frequency response on the sound pressure level and phase. The CTBTO requires their calibration in the 0.02–4 Hz frequency range.

The primary reference method routinely used in the National Metrology Institutes for sound pressure calibration is the pressure reciprocity method [7], applied at frequencies up to 25 kHz and, recently, down to 2 Hz [8]. For now, there is no primary standard and therefore no calibration capability and method in the frequency range below 2 Hz (Fig. 1).

In order to validate microbarometers' performance in a wide frequency range, a dynamic pressure infrasound generator was built by the CEA [9–11]. Over the past 10 years, this generator has been used considering a perfect linear response and constant environment variables, including some estimated first order corrections on the amplitude response. Although this use was sufficient to calibrate infrasonic sensors with a given degree of uncertainty, this generator is now in need of a more accurate characterisation. Considering that the priority is the reduction of uncertainties and regarding the fact that there are no standardised method and reference in the infrasonic domain, the next objective is to build up an acoustic primary standard in the infrasonic range based on the CEA infrasound generator technology. To understand

E-mail address: paul.vincent@cea.fr (P. Vincent)

https://doi.org/10.1016/j.apacoust.2018.12.033
0003-682X/

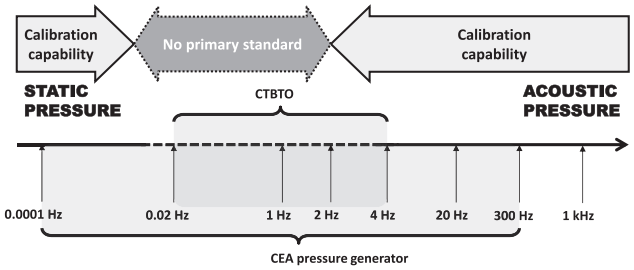

Fig. 1. Illustration of the actual state in calibration capabilities from the static pressure range to the dynamic pressure frequency range such as defined in [8].

the limitations of the generator, a complete modelling of this device appears to be an essential preliminary step.

This paper addresses two specific phenomena affecting a behaviour of an infrasound generator: the thermodynamic transition from isothermal to adiabatic transformation and the influence of the loudspeaker membrane's viscoelastic non-linearities. The amplitude and the phase response of the infrasound generator from 4.0 10^{-4} Hz to 300 Hz is presented with an analytical modelling of the sound pressure in the cylindrical cavity. A fit of this modelling on measurements is also performed with a genetic algorithm.

1.2. Infrasound generator

The CEA dynamic infrasound pressure generator is based on a pistonphone concept [12] in which the volume variation of a sealed cylinder induces a pressure variation inside it. The front sealed metallic cavity is in a vertical orientation (374-mm diameter and 270-mm high). A device under test (DUT) and a reference microphone (Mic) are coupled to the front cavity (Fig. 2). Its upper side is closed by a flat and stiff plate associated with the mobile diaphragm of a loudspeaker. This device acts as a rigid piston with an assumed perfect translation motion in a perfect cylinder. The loudspeaker, located in the back sealed cavity, is driven by a voltage that induce the piston motion. The CEA dynamic pressure generator's main characteristics are a frequency range from 4.0 10^{-4} Hz to 300 Hz, a resonance frequency at 90 Hz, and a dynamic pressure level up to 50 Pa. Fig. 2 introduces the variables describing the generator geometry: V_f and V_b are the front and back cavities volumes, S_f and S_b the corresponding vibrating surfaces, A_f and A_b the total corresponding areas, and ξ the plate displacement. P_f and P_b are the dynamic pressures of respectively the front and back cavities. The volume of the DUT is not taken into account, since it is negligible regarding V_f. Indeed, the internal volume of the DUT is about 100 times lower than V_f.

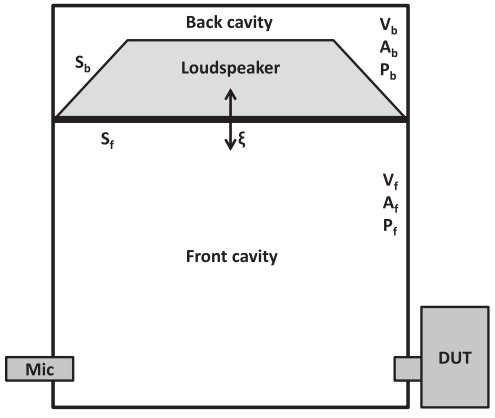

Fig. 2. Schematic illustration of the infrasound pressure generator.

2. Models

The relevant pressure is the one in the front cavity, to which sensors are coupled. In this paper, this dynamic pressure is expressed with two models: the first one is under adiabatic assumption, the second one is a global model that is based on the assumption of a uniform pressure only. The main difference is that the global model takes into account the transition of the thermodynamic transformation from isothermal to adiabatic condition.

2.1. Expression of the displacement

Using Newton's second motion law, the displacement field of the plate, which is considered to be uniform when assuming a 1-degree of freedom movement, can be expressed in a steady-state sinusoidal regime as

$$-m\omega^2\xi = Bl\,i - j\omega h\xi - K\xi + mg - S_fP_f + S_bP_b, \tag{1}$$

with ω the angular frequency [rad·s^{-1}], ξ the displacement of the plate [m], Bl the force factor of the loudspeaker [T·m], i the electric current injected in the loudspeaker coil [A], h the fluid friction [N·s·m^{-1}], K the membrane stiffness [N·m^{-1}], mg the gravity force [N] on the membrane with a mass m [kg], and S_fP_f and S_bP_b the pressure forces [N] respectively on the front and on the back sides of the membrane. Some of these parameters are shown on Fig. 2. The electric current i could be written with the generalized Ohm's law as

$$i = \frac{U - j\omega Bl\,\xi}{R + j\omega L}, \tag{2}$$

where U is the voltage applied to the loudspeaker terminals [V], R the coil electrical resistance [Ω], and L the coil's inductance [H].

2.2. Loudspeaker non-linearities

The modified flat plate used in this device increases the non-linear effects of the loudspeaker behaviour. Considering the low frequency range, it is important to take into account a creep phenomenon that arises from visco-elastic properties of the loudspeaker suspension and prevents it behaving as a simple stiffness. Several works on the loudspeakers non-linear stiffness have been carried out [13,14]. More specifically, Ritter and Agerkvist [15] described the non-linear stiffness model $K = K(\omega)$ as

$$K(\omega) = K_0\left[1 - \alpha\log_{10}\frac{j\frac{\omega}{\omega_0}e^{-j\tan^{-1}\left(\frac{\omega}{\omega_0}\right)}}{\sqrt{1+\left(\frac{\omega}{\omega_0}\right)^2}}\right]^{-1}, \tag{3}$$

where K_0 is the usual stiffness [N·m^{-1}], α is the creep factor, and ω_0 can be interpreted as the frequency where the creep of the suspension starts to rise [rad·s^{-1}]. This model expresses a behaviour where the stiffness is constant when $\omega > \omega_0$ and decreases when the frequency decreases. Thus, the pressure field in the cavity can be expected to increase when the frequency decreases, characterised by a fixed slope when plotted logarithmically, especially in the infrasound domain when $\omega \ll \omega_0$.

As far as the displacement of the plate remains relatively low in comparison with the distortion due to high level amplitude, the non-linearity of the force factor $Bl = Bl(\xi)$ is not taken into account here, though, numerous works on this phenomenon have been carried out [16,17]. Thus, not all the non-linearities of the loudspeaker have been taken into account. The present work has focused on a low amplitude level, which already seems to be sufficient to observe and model behaviour of the system.

2.3. Model with adiabatic assumption

The easiest way to express the pressure in a cavity is to consider an adiabatic transformation, as used in a usual acoustic problem. The first law of thermodynamics gives the relation between the dynamic pressure p in a volume V for a perfect gas as

$$\frac{p}{P_0} + \gamma \frac{\delta V}{V} = 0, \tag{4}$$

$$p = -\frac{\gamma \delta V}{\chi_T V}, \tag{5}$$

where $\delta V = \int \int_S \xi . \mathrm{d}S = S\xi$ is the variation of the volume V due to the movement ξ of the plate of surface S, γ being the specific heat ratio, and $\chi_T = -1/V\,(\partial V/\partial P)_T$ the isothermal compressibility coefficient. For a perfect gas, $\chi_T = 1/P_0$. In the case of the infrasound pressure generator,

$$P_f = \frac{\gamma S_f}{\chi_T V_f}\,\xi \quad \text{and} \quad P_b = -\frac{\gamma S_b}{\chi_T V_b}\,\xi. \tag{6}$$

This solution for the pressures in the front and in the back cavities (Fig. 2) is valid considering a perfect gas under the adiabatic assumption. The operating frequency range of the CEA infrasound generator does not validate the adiabatic hypothesis, therefore the isothermal to adiabatic thermodynamic transition have to be considered.

2.4. Global model with isothermal to adiabatic transition

As Fletcher [18] explained, the operating frequency range of the generator does not justify the adiabatic assumption. His reasoning is to write the lowest frequency f_a which validates adiabatic hypothesis as

$$f_a \gg \frac{\lambda}{2r^2}, \tag{7}$$

where λ is the thermal diffusivity ($\lambda = 2.11\,10^{-5}\mathrm{m}^2 \cdot \mathrm{s}^{-1}$ for air at standard conditions) and r a characteristic dimension. Taking $r = 0.01$ m as the effective radius of an equivalent sphere for the back cavity of the CEA generator with the loudspeaker in it, this adiabatic assumption approximation becomes

$$f_a|_{\text{back cavity}} \gg 1.0\ 10^{-3}\ \text{Hz}. \tag{8}$$

Therefore, it seems that the isothermal effects begin to be important for frequencies lower than 10^{-2} Hz. Then, it is necessary to take into account the isothermal to adiabatic thermodynamic transition. The effects of the thermal conduction in an acoustic wave have been theoretically described by Daniels [19] and Golay [20] for simple geometries such as a sphere, a rectangular cavity, or an infinite cylindrical cavity.

Considering small amplitude disturbances of the fluid (air), the homogeneous equations can be linearised. Taking into account the thermodynamic law expressing the density variation as function of the independent variables p and τ (being respectively the dynamic pressure and the dynamic acoustic temperature shift), the conservation of mass equation, can be written as

$$\iiint_V \left(\nabla \cdot v + \chi_T \frac{\partial}{\partial t}(p - \beta\tau) \right) \mathrm{d}V = 0, \tag{9}$$

with v the particle velocity, and $\beta = (\partial P/\partial T)_V$ the increase in pressure coefficient per unit of increase in temperature at constant volume [Pa·K^{-1}].

The infrasound generator chamber is assumed to be rigid apart from the moving loudspeaker plate. In the Fourier domain, the previous equation becomes

$$\left(1 - \frac{\beta}{p}\langle\tau\rangle\right) p = -\frac{\delta V}{\chi_T V}, \quad \text{with } \langle\tau\rangle = \frac{1}{V}\iiint_V \tau \mathrm{d}V. \tag{10}$$

Even if τ changes significantly within the boundary layers, it is interesting to see that the dynamic pressure only depends on the volumetric averaging of the temperature variation $\langle\tau\rangle$, induced by the dynamic pressure variation p.

Guianvarc'h et al. [21,22] presented a formulation to express $\langle\tau\rangle$ in a closed cylinder originally developed by Gerber [23]. The volumetric averaging of this solution in the Fourier domain can be written as

$$\begin{aligned} \frac{\beta}{p}\langle\tau\rangle &= \frac{8}{\pi^2}\frac{\gamma - 1}{\gamma}\sum_{m=0}^{+\infty}\sum_{n=1}^{+\infty} D(m,n)\,E(m,n), \\ D(m,n) &= \frac{1}{(m + 1/2)^2 \lambda_n^2}, \\ E(m,n) &= \frac{1}{1 + \dfrac{\lambda_n^2 R^2 + (m + 1/2)^2 \pi^2}{(1 + 2R)^2}\dfrac{A^2}{V^2}\dfrac{c_0 l_h}{j\omega}}, \end{aligned} \tag{11}$$

where λ_n corresponds to the zeros of integer-order $J_n(x)$ Bessel function, $R = l/(2a)$ is the ratio of the length over the radius of a perfect closed cylinder and $l_h = \lambda/(\rho_0 c_0 C_p)$ is a characteristic thermal length as defined in [24]. This equation is used in an approximated developed form in reciprocity calibration of microphones used to establish acoustic primary standards [7]. However, the entire solution (11) is required for the CEA generator because of the very low frequency domain.

A complex corrected heat capacity ratio can then be written to take into account the thermodynamic effects in a closed cylindrical cavity, with c standing for the front ($c = f$) or the back ($c = b$) cavity,

$$\gamma'_c = [1 - \beta/p\,\langle\tau\rangle_c]^{-1}. \tag{12}$$

Fig. 3 shows an example of the thermodynamic transition from an isothermal transformation to an adiabatic transformation in the CEA generator. In the lowest frequency range, $|\gamma'| = 1$, which is equivalent to an isothermal one. In the highest frequency range, $|\gamma'| = 1.4$, which is equivalent to an adiabatic transformation.

Hence a more accurate than Eq. (6) expression relating P_c and ξ,

$$P_c = \frac{\gamma'_c S_c}{\chi_T V_c}\,\xi. \tag{13}$$

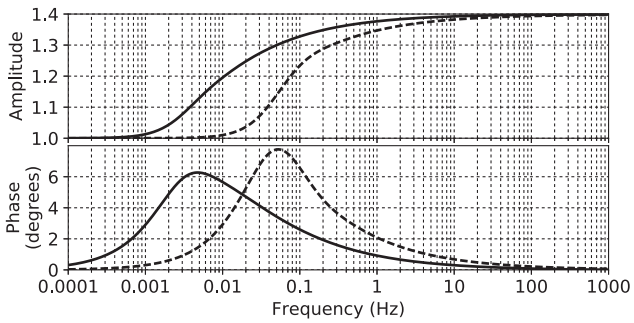

Fig. 3. Amplitude and phase of the complex corrected heat capacity ratio γ'_c taking into account the thermodynamic effects in the cavities (– for the front cavity, - - for the back cavity) over frequency variation from 10^{-4} Hz to 10^3 Hz.

2.5. Pressure in the front cavity

The relevant pressure is the one in the front cavity, to which sensors are coupled. Using (1), (2), (3) and (13), the global model of this pressure variation can by the end be written as

$$P_f(\omega) = \frac{\left(\frac{BlU}{R+j\omega L} + mg\right)\frac{\gamma_f S_f}{\chi_T V_f}}{K(\omega) + j\omega h + \frac{j\omega (Bl)^2}{R+j\omega L} - m\omega^2 + \Psi_c}, \quad \text{with } \Psi_c = \sum_{c=b,f} \frac{\gamma_c S_c^2}{\chi_T V_c}. \tag{14}$$

In the case of an adiabatic model, one must consider the classical specific heat ratio $\gamma_f = \gamma_b = \gamma$ ($\gamma = 1.4$ for dry air at 20 °C).

In the case of the global model, one must consider the corrected heat capacity ratios $\gamma_f = \gamma'_f$ and $\gamma_b = \gamma'_b$ as defined in (12).

The major difference between the two models is that the global one takes into account the thermodynamic transition from an isothermal transformation to an adiabatic one.

A preliminary study was carried out before the work was completed. The idea was to remove the rear cavity of the infrasonic dynamic pressure generator, in order to add a new dimension to the understanding of the system. This approach has made it possible to eliminate in the model the complex phenomena that appear in the rear cavity. This first study confirmed the usefulness of working with the modelling presented in this article.

3. Measurements

The aim of the CEA infrasound generator is the characterisation and calibration of infrasound sensors, *e.g.* microbarometers. In order to achieve an infrasound primary standard in a near future, the CEA generator appears to be an appropriate system to observe the phenomena that occur in the infrasound frequency range. This section presents the measurements of this system response. In Section 4.3, the measured amplitude and phase of the pressure are then compared to the models detailed in the previous section.

3.1. Setup

The measurements were carried out with a B&K 4193-L-004 microphone calibrated by the laser pistonphone of the National Physical Laboratory [12] and an MB2000 microbarometer. The first order low-frequency high-pass filter of the microbarometer has been modified to get a −3 dB cut-off frequency at 10^{-3} Hz and therefore to have a better signal-to-noise ratio. Its response is based on its theoretical modelling [25,26] and the measurement of its electrical components. The calibrated B&K 4193-L004 microphone is used for the frequency points from 10 Hz to higher frequencies, and the microbarometer for the ones from 10^{-4} Hz up to 10 Hz. Going down at such low frequencies is a choice made to explore the fully isothermal area of the system, and therefore test the models. These very low frequencies are not usually used with this generator.

Fig. 4 presents a diagram of the driving and control system. The signal generation and acquisition are driven by a VTI Instruments CMX09 chassis with an EMX-1434 waveform generator and two EMX-4350 24-bit digitizers. The generated signal is amplified by an AE TECHRON 7224 DC-enabled AC amplifier and both sent to the loudspeaker and digitised by the EMX-4350. A relay card SMX-2002 commands two solenoid valves to equalize the static pressure between the cavities in the case of a significant pressure

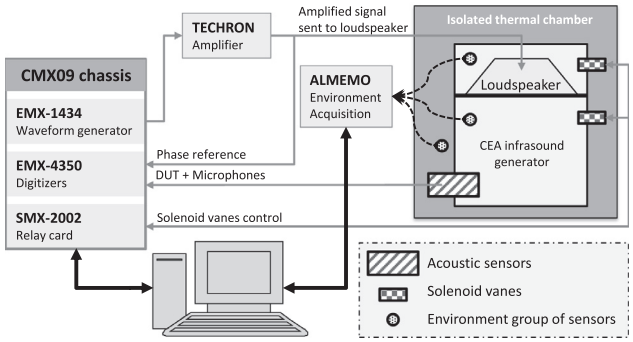

Fig. 4. Schematic illustrations of the experimental set up of the driving and control system.

variation. During the measurement, an ALMEMO 5690-1M environmental acquisition system digitises a dozen of temperature, hygrometry and static pressure sensors. These sensors are located inside and outside the cavities, on the surfaces of the infrasound generator and in the air. The CEA generator and its sensors are located inside an isolated thermal chamber which reduces significantly the ambient temperature variations.

The control and command software (written in Python language) is designed to remain stable for up to several weeks which is the period required for a long measurement campaign.

3.2. Frequency points

For each chosen frequency points of interest, a sinusoidal signal is generated several times by the driving and control system in order to compute repeatability uncertainties. The duration of the measurement directly depends on three parameters: the chosen frequency range, the number of points of interest and the number of periods needed for each generated point. The lower the frequency, the longer the measurement duration.

3.3. Amplitude and Phase

The amplitude (in dB re. 1 V) and the phase (in degrees) are estimated by a projection of digitised sensor signals on the sinus basis, inspired by IEEE Standard 1057:2017 [27], as explained thereafter. In order to fit a digitised sinusoidal waveform signal $y(t) = \underline{Y_d}$ to a sine wave in the case when the frequency f_g and the temporal basis t are known,

$$\underline{Y_d} = A\sin(2\pi f_g t + \phi), \tag{15}$$

and the unknown parameters are its amplitude A and its absolute phase delay ϕ.

The $\underline{Y_d}$ signal is truncated to get a whole number of periods, based on f_g frequency. This equation can be decomposed as

$$\begin{aligned} \underline{Y_d} &= B\cos(\phi)\sin(2\pi f_g t) + C\sin(\phi)\cos(2\pi f_g t) \\ &= D\underline{S_1} + E\underline{S_2}, \end{aligned} \tag{16}$$

where the unknown scalars are $D = B\cos(\phi)$ and $E = C\sin(\phi)$, the known vectors are $\underline{S_1} = \sin(2\pi f_g t)$ and $\underline{S_2} = \cos(2\pi f_g t)$.

Using the transposed known vectors $\underline{S_1}^T$ and $\underline{S_2}^T$, the projection of the signal on the sinus basis at the f_g frequency gives,

$$\begin{aligned} &\begin{cases} \underline{S_1}^T\underline{Y_d} &= D\underline{S_1}\underline{S_1}^T + E\underline{S_2}\underline{S_1}^T \\ \underline{S_2}^T\underline{Y_d} &= D\underline{S_1}\underline{S_2}^T + E\underline{S_2}\underline{S_2}^T \end{cases} \\ \Longleftrightarrow\ &\begin{cases} S_{1Y} = DS_{11} + ES_{21} \\ S_{2Y} = DS_{12} + ES_{22} \end{cases}. \end{aligned} \tag{17}$$

Since $S_{12} = S_{21}$,

$$\begin{cases} D &= \dfrac{S_{1Y}S_{22} - S_{2Y}S_{12}}{S_{11}S_{22} - S_{12}S_{12}} \\ E &= \dfrac{S_{2Y}S_{11} - S_{1Y}S_{12}}{S_{22}S_{11} - S_{12}S_{12}} \end{cases}. \tag{18}$$

Then, the amplitude A and the phase ϕ can be written as

$$\begin{aligned} A &= \sqrt{D^2 + E^2} \text{ and} \\ \phi &= \arctan\left(\tfrac{E}{D}\right). \end{aligned} \tag{19}$$

3.4. Static pressure equalization

Since the measurements last several days to go down to $4.0\ 10^{-4}$ Hz due to low frequencies points and repeatability, the external static pressure can vary up to ±20 hPa around the initial value. Since the cavity is full sealed, it has been observed that the CEA generator is sensitive to the static pressure variation. In order to reduce this effect an equalization of the internal and external static pressures is made between each generated point, this is done by the use of solenoid valves controlled by the software through a relay card. The amplitude of the external static pressure variation between two equalizations can reach up to 5 hPa at very long frequency points.

3.5. Temperature variations

The temperature in the laboratory varies around 23 ± 2 °C. Since the CEA generator and the sensors are sensitive to temperature variations, they are placed in an insulated box used to reduce the amplitude of temperature variations. The effect of this box is to reduce these variations by a factor of 10 around the generator, and then to reduce these variations by a factor of 100 inside the closed front cavity where the sensors are coupled. The measurement starts when the overall thermal balance is achieved.

4. Optimization and fit

4.1. Genetic algorithm

Actually, the model given in (14) uses a lot of hard-to-measure or unknown parameters, such as the α creep factor, the fluid friction h, the mobile membrane mass m or the total areas A_c. The difficulty is to find the model parameters that fit the measurements both in amplitude and phase. As there are up to 17 interdependent parameters that drive the model, classical optimization algorithm cannot properly converge. In fact, it was observed in this case that the arbitrary origin, chosen to start a classical constrained minimization method, impacts the fitting result.

To compensate for that, a Genetic Algorithm (GA) has been adapted from [28]. The main property of an evolutionary algorithm is that the problem's origin can be randomly chosen. Each launch starts from a new randomly chosen origin but considering a sufficient number of iterations it should end up with the same final result. Also, the propagation of the algorithm follows a chosen probabilistic law for each parameter.

GA are based on the evolution of a population in an environment as explained, for example, in [29]. The general principle is to make individuals survive in a hostile environment. The individuals with the best genome will be the only ones left alive at the end of the process. By analogy, in this study, an individual characterised by its genome corresponds to one set of the 17 independent parameters that drive the model (14). The hostile environment corresponds to the measurements of the amplitude and phase of the infrasound generator presented in Section 3, with which the individuals are compared through the model. The aim of the evolutionary process is to find the set of parameters that best fits the model to the measurements (*i.e.* the best genome that survives to the environment). Fig. 5 shows a diagram describing the evolutionary process in search of the best set of parameters.

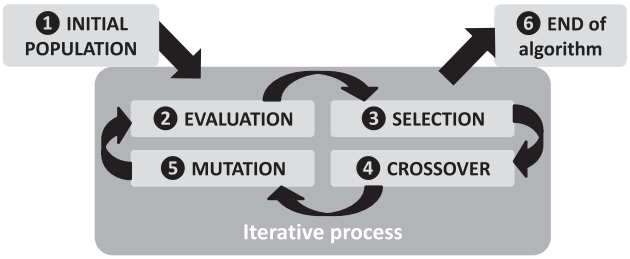

Fig. 5. Schematic diagram of the evolutionary process.

1. The first step is the initialization of the population. Each individual is characterised by his genome. In the present study, a genome corresponds to a random set of the 17 independent parameters. The coding of the parameters was done according to a bounded array and normalised to the unit. This is a usual direct value encoding method for real numbers. The genome attribution follows a uniform law bounded by the description of the parameters. The population size (*i.e.* the number of individuals) is chosen to minimize calculation cost and maximize convergence. For the present experiment, 500 individuals have randomly been generated (*i.e.* 500 sets of genomes). The iterative process can then begin.
2. The evaluation step calculates the model result (14) with the genome of each individual. The model is launched with each genome set of parameters, which gives an amplitude level and phase response for each individual of the population. Survival to the environment corresponds to testing the closeness of the model to the measurements. The evaluation is done by an objective function calculating an arbitrary fitness value, which is an image of this closeness, explained in the following.
3. The population evolves by selection: only the most adapted individuals in the environment survive. For the present study, this corresponds to keeping only the parameter sets that produce with the model (14) the amplitude and phase results closest to the measurements of the infrasound generator response. To select individuals among themselves, their fitness values are compared. The lower this fitness value, the better the set of parameters found. Some of the best individuals from the former population are selected by a random 4-individual-size tournament selection [29]. This method allows to keep in the process genomes with parameters that could be correct even if the global result of the model is far from the measurements.
4. At each population generation, several individuals are crossed according to a probabilistic criterion (chosen to minimize process time and maximize convergence, in this study p = 0.7). The crowding degree of the mutation is 0.1, this produce a mutant with some differences compare to its parents. The sequence value for the bound of the search space is chosen larger than the description of the parameters ([−5, 5]). Children are made with a two-point crossover [29], which permits mixing genome sequences. This steps swaps some parameters between individuals.
5. Some children born from the crossover are mutated, with another probabilistic criteria (in the present case p = 0.15). Several parameters mutate, following a polynomial bounded law, with a probability p = 0.25 for the apparition of formally new independent parameters.

6. The algorithm stops when a given number of generation is reached (chosen to minimize calculation cost and maximize convergence).

The optimization algorithm is written in Python language. The selection step is parallelized in order to reduce the calculation cost. Each new launch starts from a random new set of parameters and the experiment shows that they converge sensitively to the same result presented on Table 1.

4.2. Barycentered fit

The first step of the optimization is to determine some approximated values and boundaries for each parameter. The volumes V_c, the electric resistance R, the tension U and the vibrating surfaces S_c are measured.

A parametric study has shown the frequency areas where each parameter has a significant influence (thermodynamic zone, viscoelastic loudspeaker non-linearities zone, resonance zone, or a significant influence over the full frequency range). Considering the influence areas presented in Table 2, some weights must be chosen in order to balance the optimization for each area. This step allows to achieve better results in less computation time.

The bold-written parameters in Table 2 highlight the ones which have an important influence on several areas. These have to be properly chosen in order to ensure the confidence on the final result. Table 1 gives, in the column *Expected*, the estimated or measured values for the 17 parameters set of the global model. The values presented in this column are approximate estimates. For example, the dimensions of vibrating surfaces are difficult to characterise. As explained above, since the loudspeaker is modified to behave like a piston-cylinder, the addition of a honeycomb and a neoprene membrane makes it difficult to estimate some values. Their variability range takes these uncertainties into account in the algorithm.

The arbitrary errors between the measurement and the model on the amplitude (err_{amp}) and on the phase (err_{phi}), can be written as the concatenation of three weighted differences frequency bands:

$$\begin{aligned} err_{amp} &= p_{11} D_a^{[TH]} \oplus p_{12} D_a^{[NL]} \oplus p_{13} D_a^{[RE]}, \\ err_{phi} &= p_{21} D_p^{[TH]} \oplus p_{22} D_p^{[NL]} \oplus p_{23} D_p^{[RE]}, \end{aligned} \tag{20}$$

where the vectors $D_a = [measurement - model]$ and $D_p = [measurement - model]$ give the differences between measurement and model, respectively for the amplitude modulus and for the phase values. The scalar weights p_{ij} associated with the three areas $[f \in TH]$ (thermodynamic area), $[f \in NL]$ (non-linearities area) and $[f \in RE]$ (resonance area) allow to equilibrate the minimization. The matrix p_{ij} is presented in (21).

$$p_{ij} = \begin{bmatrix} 4 & 3 & 1 \\ 3 & 1 & 5 \end{bmatrix}. \tag{21}$$

As for a classical constrained minimization method, a chosen scalar to minimize δ_m, which is here the fitness value for the GA, composed by the arbitrary errors, can be written as:

$$\delta_m = p_1 \sqrt{\sum \left(err_{amp}\right)^2} + p_2 \sqrt{\sum \left(err_{phi}\right)^2}, \tag{22}$$

with the arbitrary weights p_1 [(dB Pa)$^{-1}$] and p_2 [deg^{-1}] chosen to equilibrate the unit range difference between the amplitude [dB Pa] and the phase [deg] errors. The objective is to approach a situation where 0.05 dB error in amplitude weights the same as 1 deg error in phase: $p_1/p_2 \approx 50$.

Fixing the most measurable values (S_c, V_c, U, R), several launches of the genetic algorithm are made with a uniform and bounded probabilistic law for the other parameters. This step gives a first estimation of the model's parameters. At this point, a more accurate estimation is needed. A Monte Carlo uncertainties propagation [30] is made to get a standard deviation of the model on the whole frequency range. The uncertainty range is chosen as a uniform law from 0.1% variation for the measured U value, to 90% variation for the unknown R_b value.

Considering the weights and the standard deviation on the amplitude std_{amp} and the phase std_{phi}, the scalar minimizer becomes

Table 2
Global model significant influence areas for each parameter. TH, NL, RE, Full respectively stand for THermodynamic area, viscoelastic loudspeaker Non-Linearities area, loudspeaker REsonance area, and Full frequency influence zone in amplitude and phase.

TH <0.01 Hz	NL [0.01–10] Hz	RE ≈90 Hz	Full [10^{-4}–300] Hz
A_c	ω_0, α	ω_0, α, L, h	
R_c	$\mathbf{K_0}$	$\mathbf{K_0}$	$\mathbf{K_0}$
$\mathbf{V_c}$		$\mathbf{V_c}$, $\mathbf{S_c}$	$\mathbf{V_c}$, $\mathbf{S_c}$
		m, **Bl**	**m**, **Bl**

Table 1
Global model parameters used to characterise the infrasound pressure generator.

Name	Parameter	Expected	Fit	Error
Loudspeaker voltage	U [V]	$= 3.27$		
Coil resistance	R [Ω]	$= 14.5$		
Coil inductance	L [H]	$\approx 10^{-2}$	1.13 10^{-2}	2.7%
Force factor	Bl [T·m]	≈ 28.8	28.4	1.3%
Membrane mass	m [kg]	$0.3 < m < 0.6$	0.579	
Fluid friction	h [Ns·m^{-1}]	> 0	57.1	
Front cavity volume	V_f [m^3]	≈ 0.0328	0.03292	0.4%
Back cavity volume	V_b [m^3]	≈ 0.0145	0.01457	**0.5%**
Front vibrating surface	S_f [m^2]	≈ 0.06	0.056	6.7%
Back vibrating surface	S_b [m^2]	≈ 0.06	0.069	13%
Front total surface	A_f [m^2]	≈ 1.1	1.15	4.3%
Back total surface	A_b [m^2]	≈ 1.1	1.14	3.5%
Stiffness	K_0 [N·m^{-1}]	$10^4 < K_0 < 10^6$	1.43 10^5	
Creep pulsation rise	ω_0 [rad·s^{-1}]	>10	116	
Creep parameter	α	$0 < \alpha < 1$	0.095	
Front cylindrical ratio	R_f	≈ 0.698	0.7	2.9%
Back cylindrical ratio	R_b	>0	3.4 10^{-4}	

$$\delta_m = p_1\sqrt{\sum\left(\frac{err_{amp}}{std_{amp}}\right)^2} + p_2\sqrt{\sum\left(\frac{err_{phi}}{std_{phi}}\right)^2}. \quad (23)$$

4.3. Results and discussion

The measurements and final analytical model results are presented in Fig. 6 and the values of the parameters in Table 1. The measurements lasted 5 days with almost constant environmental variables. The fitting calculus took several days on a parallel computer first to evaluate the best area weights and evolutionary algorithm law constants and then to find the model parameters and converge at each execution. The final Monte Carlo uncertainty propagation was made on 10^5 cases.

The columns *Fit* and *Error* on Table 1 show a good correlation between expected or calculated parameters and the global model fitted parameters. The volumes shift is less than 1% error. The results presented on Fig. 6 allow to validate a model over measurements on almost 6 decades, for the amplitude level (dB Pa Ref. 1 Pa) and the phase deviation (degrees). Outside the resonance area, where a very slight frequency offset in the model induces a very large difference with the measurements, the maximum deviation between the global model and the mean of the measured data is 0.15 dB and 1 degree. As expected in Eq. (8), the adiabatic model is no more valid under 0.03 Hz both in amplitude level (deviation >0.2 dB) and phase (deviation >1 degree). This effect induces almost a 2 dB deviation between the two models at 10^{-4} Hz. Several papers already observed the deviation induced by this thermodynamic transition on sensors [31,32]. The present study presents these effects on the infrasound generator, used to calibrate the sensors. Also, the −0.4 dB/decade slope that appears on measurements below 10 Hz is strongly taken into account in the loudspeaker creep non-linearity model (3), as suggested by [13,14]. Indeed, the measurement of the displacement of the plate by interferometry in the frequency band of the phenomenon shows a very good correlation with the Ritter and Agerkvist [15] non-linearity model. This model was chosen to respond to observations of the system's behaviour both on amplitude and phase. A simpler model such as the "EXP" reference model [14] does not adequately explain the phase behaviour at high frequencies.

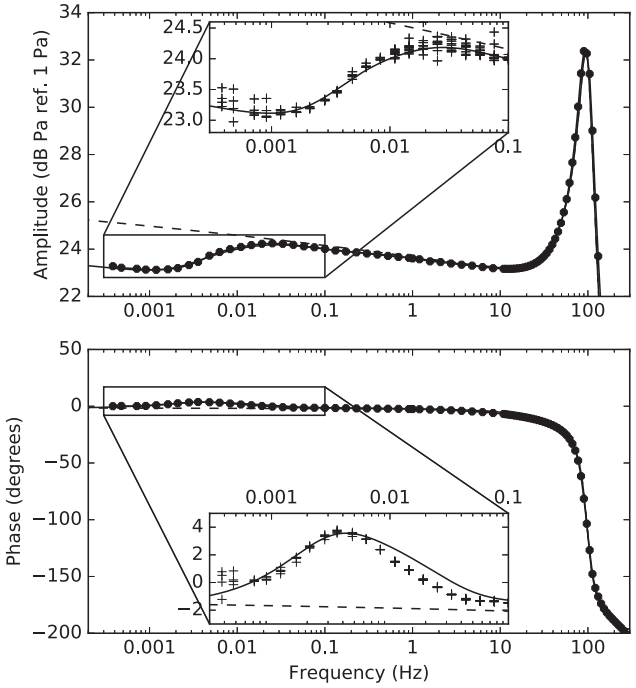

Fig. 6. Measurements and analytical models of the dynamic pressure amplitude (dB ref 1 Pa) and phase (degrees), as function of the frequency, in the front cavity of the CEA infrasound generator. The dot curve (•) is an average of measurements, the plus curve (+) corresponds to the repeated measurement points, the solid (–) and the dashed (- -) lines are respectively the global model (14) and the adiabatic model (6).

However, the developed model has several limitations. The solution for the volumetric average of the acoustic temperature (11) is valid for a perfect, closed, cylinder. In reality, the cylinders of the CEA infrasound generator are not perfect, especially for the back cavity where the loudspeaker stands. In order to compensate this non-cylindricity, the R_b parameter, normally standing for the ratio between the length and the radius, is used as a small compensation parameter. This non-cylindricity solution has only a slight impact on the results. In the high frequency range, this model does not take into account either the effects related to the volume of the DUT, or the geometry of its coupling system with the front cavity. Also, using a 17-parameter modelling complicates the independent verification of each parameter, especially if some of them are not measurable. Finally, the fact that only a theoretical response of the microbarometer is taken as reference to estimate the value of parameters below 10 Hz does not allow the result of this model to be used as a reliable source for sensor calibration. Other unknown and unaccounted for effects may be composed in somehow by coincidence. Indeed, this theoretical response is not a traceable metrological reference as such. However, such a possibility seems unlikely, since the phase response does not diverge at low frequencies and remains very flat compared to the conventional behaviour of the sensor. Nevertheless, the traceability of measurements in the infrasonic frequency range is an essential element on which future work will have to provide answers.

5. Conclusion

The aim of this work was to find a more accurate characterisation of the CEA infrasound generator in order to make measurements with infrasound sensors more reliable. The model and the measurements presented in this paper reflect the generator behaviour down to 4.0 10^{-4} Hz and validate a 17-parameters fit with a slight deviation in amplitude and phase. These results provide the opportunity to consider mechanical improvements of the system with the understanding of the physical phenomena at stake. They also improve confidence in the measurements done with this equipment.

For future generator manufactures, particular attention may be paid to the choice of the membrane stiffness, the cavity volume, and the resonance frequency of the global system, since this study indicates that these quantities play a major role in the behaviour of the infrasound generator over its entire operating frequency range.

This work allows the transformation of a volume variation model into a dynamic pressure variation model to be tested for the first time on the CEA infrasound generator. In order to validate this model at the level of a normative requirement, independent tests must be carried out, with a limited number of parameters and a complete control of them. In the future, the interferometric measurement of the plate displacement, chosen as a reference, will no longer need so many parameters.

The purpose of future work is now, in the short term, to design a primary standard generator in the infrasonic frequency range, in accordance with the BIPM strategy [33].

Appendix A. Supplementary data

Supplementary data associated with this article can be found, in the online version, at https://doi.org/10.1016/j.apacoust.2018.12.033.

References

[1] Le Pichon A, Herry P, Mialle P, Vergoz J, Brachet N, Garcés M, et al. Infrasound associated with 2004–2005 large sumatra earthquakes and tsunami. Geophys Res Lett 2005;32.

[2] Fee D, Matoza RS. An overview of volcano infrasound: From hawaiian to plinian, local to global. J Volcanol Geoth Res 2013;249:123–39.

[3] Leventhall G. Infrasound from wind turbines-fact, fiction or deception. Can Acoust 2006;34:29–36.

[4] Schimmel A, Hübl J, Koschuch R, Reiweger I. Automatic detection of avalanches: evaluation of three different approaches. Nat Hazards 2017;87:83–102.

[5] NF XP S 31-135, Acoustique - Basses fréquences - Méthode de mesurage, Standard, NF XP S 31-135, 2017.

[6] DIN 45680:1997–03, Messung und Bewertung tieffrequenter Gerausschimmissionen in der Nachbarschaft, Standard, DIN 45680:1997–03, 1997.

[7] International Electrotechnical Commission, et al., IEC 61094–2: 2009, Measurement microphones-Part2: Primary method for the pressure calibration of laboratory standard microphones by the reciprocity method (2009).

[8] BIPM, Acoustics, Ultrasound and Vibration - Calibration and measurement capabilities, 2018 (accessed June 29, 2018).URL: http://kcdb.bipm.org/AppendixC.

[9] Larsonner F, Uszakiewicz H-G, Mende M. Infrasonic sensors and their calibration at low frequency. INTERNOISE and NOISECON Congress and Conference Proceedings, vol. 249. Institute of Noise Control Engineering; 2014. p. 1127–36.

[10] Larsonnier F, Millier P. Un dispositif original pour la métrologie acoustique basse fréquence appliquée aux capteurs d'infrasons. Acoust Techn 2011:17–23.

[11] Alcoverro B. Infrasound sensor dynamic calibrator. Hawai: Infrasound Technology Workshop; 2001.

[12] Barham R, Goldsmith M. The application of the NPL laser pistonphone to the international comparison of measurement microphones. Metrologia 2007;44:210.

[13] Maillou B. Caractérisation et identification non-paramétrique des non-linéarités de suspensions de haut-parleur Ph.D. thesis. Le Mans; 2015.

[14] Knudsen MH, Jensen JG. Low-frequency loudspeaker models that include suspension creep. J Audio Eng Soc 1993;41:3–18.

[15] Ritter T, Agerkvist FT. Modelling viscoelasticity of loudspeaker suspensions using retardation spectra.

[16] Erza M, Lemarquand G, Lemarquand V. Distortion in electrodynamic loudspeakers caused by force factor variations. Arch Acoust 2011;36:873–85.

[17] Merit B, Lemarquand V, Lemarquand G, Dobrucki A. Motor nonlinearities in electrodynamic loudspeakers: modelling and measurement. Arch Acoust 2009;34:579–90.

[18] Fletcher N. Adiabatic assumption for wave propagation. Am J Phys 1974;42:487–9.

[19] Daniels FB. Acoustical impedance of enclosures. J Acoust Soc Am 1947;19:569–71.

[20] Golay MJ. Theoretical consideration in heat and infra-red detection, with particular reference to the pneumatic detector. Rev Sci Instrum 1947;18:347–56.

[21] Guianvarc'h C, Durocher J-N, Bruneau M, Bruneau A-M. Improved formulation of the acoustic transfer admittance of cylindrical cavities. Acta Acust united with Acustica 2006;92:345–54.

[22] Guianvarc'h C. La cavité de couplage acoustique dans la méthode de réciprocité: modèles analytiques pour l'étalonnage des microphones et la mesure d'impédances de petits composants Ph.D. thesis. Le Mans; 2005.

[23] Gerber H. Acoustic properties of fluid-filled chambers at infrasonic frequencies in the absence of convection. J Acoust Soc Am 1964;36:1427–34.

[24] Bruneau M, Herzog P, Kergomard J, Polack J. General formulation of the dispersion equation in bounded visco-thermal fluid, and application to some simple geometries. Wave Motion 1989;11:441–51.

[25] Alcoverro B, Le Pichon A. Design and optimization of a noise reduction system for infrasonic measurements using elements with low acoustic impedance. J Acoust Soc Am 2005;117:1717–27.

[26] Starovoit Y, Kunakov V, Martysevich P. About the dynamical calibration of microbarometers in ims infrasound network. EGU General Assembly Conference Abstracts, vol. 11. p. 13787.

[27] IEEE 1057:2017, Standard for Digitizing Waveform recorders, Standard, IEEE, 2017.

[28] Fortin F-A, De Rainville F-M, Gardner M-A, Parizeau M, Gagné C. DEAP: evolutionary algorithms made easy. J Mach Learn Res 2012;13:2171–5.

[29] Ashlock D. Evolutionary computation for modeling and optimization. Springer Science & Business Media; 2006.

[30] BIPM, IFCC, ISO, Evaluation of Measurement Data - Guide to the Expression of Uncertainty in Measurement, Joint Committee for Guides in Metrology, Technical Report, Technical Report No. JCGM 100, 2008.

[31] Marcillo O, Johnson JB, Hart D. Implementation, characterization, and evaluation of an inexpensive low-power low-noise infrasound sensor based on a micromachined differential pressure transducer and a mechanical filter. J Atmos Oceanic Technol 2012;29:1275–84.

[32] Mentink JH, Evers LG. Frequency response and design parameters for differential microbarometers. J Acoust Soc Am 2011;130:33–41.

[33] BIPM, Strategy 2017 to 2027, Consultative Committee for Acoustics, Ultrasound, and Vibration (CCAUV), Technical Report, BIPM, 2017.